Nonlinear Dyn (2023) 111:5345–5358
https://doi.org/10.1007/s11071-022-08122-x

ORIGINAL PAPER

Bilateral continuous terminal sliding mode control for teleoperation systems with high-order disturbances

Zhenhua Zhao · Ting Li · Dong Cao · Jun Yang

Received: 8 November 2021 / Accepted: 18 November 2022 / Published online: 30 November 2022

Abstract A new bilateral continuous terminal sliding mode control method is proposed to attenuate the high-order time-varying disturbance in teleoperation systems based on enhanced nonlinear disturbance observer (ENDOB). Firstly, the control task of the teleoperation systems is transformed into stabilization of the position and force tracking errors. And then, the ENDOBs are introduced to estimate the high-order lumped disturbances in position and force tracking error subsystems. Finally, based on the estimation of lumped disturbances, a bilateral continuous terminal sliding mode controller is developed. The proposed bilateral controller not only guarantees the continuity of the control action but also guarantees the position and force tracking errors converge to a small bounded region even when there exist high-order time-varying disturbances. The effectiveness of the proposed method is validated by its applications on a bilateral lift robot system.

Keywords Terminal sliding mode · Continuous sliding mode control · Nonlinear disturbance observer · High-order disturbances · Teleoperation system

1 Introduction

Teleoperation denotes the local operator manipulates objects remotely with similar conditions as those at the remote location [1]. The teleoperated robot systems extend operator's manipulation capability to remote location, and they are widely utilized in practical engineering [2], such as outer space exploration [3], minimally invasive telesurgery [4], walking robot design [5], etc. Teleoperation systems usually contain five parts (see Fig. 1): human operator and master robot in local site, slave robot and environment in remote site, and communication channel which combines local and remote sites. The ideal teleoperation systems guarantee the operator manipulates and haptic environment directly as if it were mechanically connected with environment [6].

Figure 1 demonstrates the internal signal flow of a teleoperation system: (1) the operator manipulates the master robot and leads to its displacement x_m in local site and (2) master and slave robots generate specified control actions τ_m and τ_s to guarantee the slave robot in the remote site has the same displace-

This work was supported by grants from the Natural Science Foundation of China (Nos. 62103194, 61903192), the Jiangsu provincial colleges of Natural Science General Program (21KJB120007), Basic scientific research business expenses of Central Universities (NT2021011).

Z. Zhao · D. Cao
College of Automation Engineering, Nanjing University of Aeronautics and Astronautics, Nanjing 211106, China

T. Li (✉)
School of Mathematical Sciences, Nanjing Normal University, Nanjing 210023, China
e-mail: dylliting@njnu.edu.cn

J. Yang
Department of Aeronautical and Automotive Engineering, Loughborough University, Loughborough LE11 3TU, UK

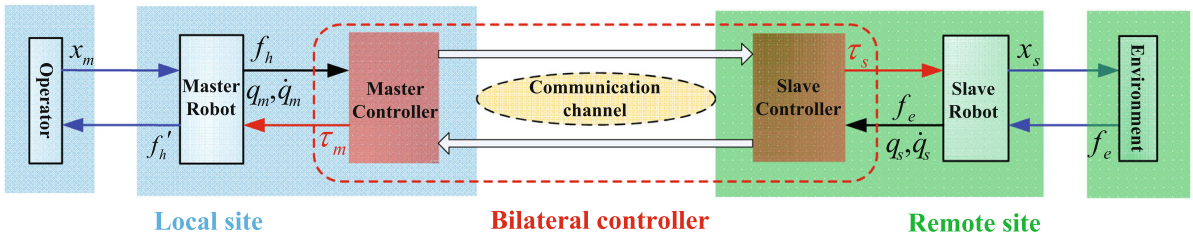

Fig. 1 Internal signal flow of a teleoperation system

ment and the master–operator contact force in the local site are the same with the slave–environment contact force. Since the information flows between local and remote environment, the control strategy for teleoperation systems is called bilateral control [7]. If the slave robot accurately reproduces the master's motion (i.e., $x_s = x_m$) and the master robot exactly displays the slave–environment contact force to human operator (i.e., $f_h' = f_e$), the ideal transparency is achieved [8].

To achieve high transparency, based on the linear models of master and slave robots, various control methods, such as the adaptive control [9], passivity-based approach [10], and acceleration-based control methods [11], have been proposed. These methods improve the position and force tracking performance when master and slave robots are free of disturbances. To deal with the influence of disturbances, the linear disturbance observer (LDOB) [12] is introduced in the bilateral controller design [13,14]. In [13], the LDOBs are designed both in master and slave robots to estimate the disturbances in them independently, and then, a composite controller is developed based on the LDOBs' estimation. In [14], the LDOBs are designed to estimate the couplings' influences between the force and position tracking error dynamics, and then, a composite bilateral controller is constructed based on the estimation. Although the above methods have improved the transparency from different aspects, they all view the nominal model of teleoperation systems as linear systems. However, robots usually have serious nonlinearity due to its mechanical configuration [15], and the control performance of teleoperation systems degrades significantly in this case.

To attenuate the influences of nonlinearity, many advanced nonlinear control methods such as finite-time control method [16], predictive control method [17], and sliding mode control method [18] have been proposed for teleoperation systems. These methods introduce the nonlinear terms into bilateral controller design in a feedback way and achieve good transparency when system model is accurate and free of disturbances. To deal with the disturbances in the teleoperation system, the nonlinear disturbance observer (NDOB) [19] is introduced in the nonlinear bilateral controller design. In [20] and [21], based on the NDOB technique, the nonlinear composite bilateral control framework is proposed for one-degree-of freedom and n-dof teleoperation systems, respectively. This nonlinear composite bilateral control framework guarantees the convergence of position and force tracking error when the teleoperation system in the presence of uncertainties and disturbances. Many advanced effective observer methods have been proposed, such as the enhanced nonlinear disturbance observer (ENDOB) [22], fixed-time observer [23], and sliding mode observer [24]; they guarantee high-precision estimation of generous time-varying disturbances. However, only the slow time-varying disturbances are considered in the existing bilateral control methods.

Due to its strong robustness against uncertainties [25], sliding mode control method has attracted wide attentions in control engineering field [26]. Considering the wide applications of sliding mode control method on practical engineering, such as the flight control systems [27], mechatronic systems [28], and also telerobotic systems [29], the sliding mode control method is employed for the bilateral controller design in this paper: a new composite continuous terminal sliding mode control method based on the ENDOB is proposed to deal with the high-order time-varying disturbances in teleoperation systems. Firstly, the control task of the teleoperation systems is transformed into stabilizing the position and force tracking errors. Secondly, the ENDOBs are introduced to estimate the high-order lumped disturbances in position and force tracking error dynamics. And then, based on the esti-

mation of the ENDOBs, the composite continuous terminal sliding mode bilateral controllers are developed both in position and force tracking subsystems. Finally, the real control actions of the teleoperation, i.e., the electrical torques of master and slave robots, are calculated based on a nonlinear transformation. Compared with the existing methods, the proposed method has the following major merits: (1) guarantee position and force tracking errors convergence to a bounded region in finite-time even in the presence of high-order time-varying disturbances and (2) guarantee the continuity of control action.

The rest of the paper is organized as follows: in Sect. 2, the model and control problem formulation of the teleoperation systems are given. Section 3 demonstrates the controller design details and also gives a strict stability analysis of the proposed method. Simulations based on the proposed method for a bilateral lift robot system are carried out in Sect. 4. Section 5 ends the paper with a conclusion.

2 Problem formulation

2.1 Model of teleoperation systems

Without loss of generality, the master and slave robots are both considered as single-degree-of-freedom actuators to simplify the deduction. Let the subscript m and s represent master and slave robot, respectively, q_m, q_s and $\dot{q}_m$, $\dot{q}_s$ denote the generalized joint positions and velocities of master and slave robots. The model of master and slave robots can be obtained as [30]:

$$\begin{aligned} &a_m(q_m)\ddot{q}_m + b_m(q_m, \dot{q}_m) + g_m(q_m) = \tau_m - \tau_{mext} - \tau_h, \\ &a_s(q_s)\ddot{q}_s + b_s(q_s, \dot{q}_s) + g_s(q_s) = \tau_s - \tau_{sext} - \tau_e, \end{aligned} \tag{1}$$

where $a_m(q_m)$ and $a_s(q_s)$ denote the inertia of master and slave robots, $b_m(q_m)$ and $b_s(q_s)$ are the internal torques due to the Coriolis and centrifugal forces, $g_m(q_m)$ and $g_s(q_s)$ are the internal torques due to the gravity force. τ_m and τ_s are the electrical torques of master and slave robots, and they are also the control input of the teleoperation system; τ_{mext} and τ_{sext} are the external unmodeled torques due to friction force or other unknown torques. τ_h and τ_e are the external torques due to the contact force, and they could be modeled as:

$$\tau_h = f_h l_m, \quad \tau_e = f_e l_s,$$

where f_h are the contact force exerted on master by operator, f_e are the contact force exerted on slave by environment, l_m and l_s are the distances between the shaft and the point where the contact force is applied. The contact force f_h and f_e is usually modeled as mass spring damper [13]:

$$\begin{aligned} &f_h = D_h(\dot{s}_m - \dot{s}_h) + K_h(s_m - s_h), \ s_h > s_m; \\ &f_e = D_e(\dot{s}_s - \dot{s}_e) + K_e(s_s - s_e), \quad s_s > s_e; \end{aligned} \tag{2}$$

with

$$s_m = q_m l_m, \quad s_s = q_s l_s,$$

where s_h, s_m, s_s, s_e are the displacements of operator, master, slave and environment, respectively; D_h, K_h, D_e, and K_e are the spring coefficients, damping coefficients of the operator, and environment. It should be noted that the contact forces f_h and f_e appear only when the contact happens (i.e., $s_h > s_m$, $s_s > s_e$). If the contact vanishes, the contact force will disappear:

$$\begin{cases} f_h = 0, \ \ if \ s_h \le s_m; \\ f_e = 0, \ \ if \ s_s \le s_e. \end{cases} \tag{3}$$

To describe the dynamics of operator and environment more intuitively, a practical teleoperation system i.e., the teleoperation lift robot system (as shown in Fig. 2) is considered in this paper, and the dynamics of operator and environment is modeled based on the lift robot system. f_h' and f_e' are contacted forces acted on the operator and environment, they are the reaction force of f_h and f_e, and they satisfy $f_h' = f_h$, $f_e' = f_e$. The dynamics of operator can be modeled as the human hands [31]:

$$\begin{aligned} M_h\ddot{s}_h = &M_h\ddot{s}_h^r + k_h(\dot{s}_h^r - \dot{s}_h) \\ &+ b_h(s_h^r - s_h) + f_h^H - f_h', \end{aligned} \tag{4}$$

where M_h, k_h, and b_h are the coefficients decided by the operator and s_h^r is the desired position of operator and f_h^H is the internal control action of operator. Since human beings can regulate the internal control action f_h^H based on the haptic of force f_h' adaptively, f_h^H can be modeled as [31]:

$$f_h^H = (1 + \lambda_h) f_h' = (1 + \lambda_h) f_h,$$

where λ_h is a feedback coefficient for the contact force. Considering the function of teleoperation lift robot system, the dynamics of environment (i.e., the body which are lifted by the slave robot) is modeled as:

$$M_e\ddot{s}_e = f_e' - M_e g = |f_e| - M_e g, \tag{5}$$

where M_e is the mass of environment object and g is the gravitational acceleration.

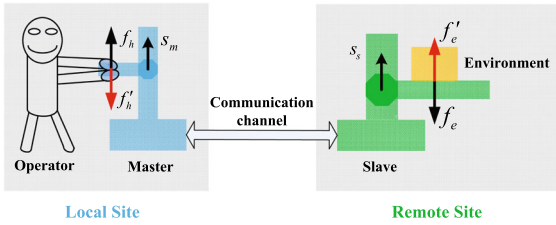

Fig. 2 Demonstration of teleoperation lift robot system

Remark 1 Considering the fact that the displacement difference between the operator and the master robot (i.e., s_h and s_m) is usually very small due to the large value of K_h in (2), the operator manipulated the master robot through transmitted its displacement s_h to s_m. As a result, the operator controls its displacement s_h by regulating its internal control action f_h^H to achieve certain movement in master robot system.

2.2 Problem Formulation

The control objective of the teleoperation system is to realize the bilateral haptic transmission between the remote side and the local side [20]. To achieve this object, the positions of master and slave robot should be the same and the contact force between human and master f_h with that between slave and environment should be the same:

$$s_m - s_s = 0, \quad f_h + f_e = 0. \tag{6}$$

Define the position tracking error of master and slave robots as e_P, the contact force tracking error as e_F. The values of e_P and e_F can be calculated as:

$$e_P = s_m - \alpha s_s, \quad e_F = f_h + \beta f_e, \tag{7}$$

where α and β are two positive scaling constants, and they are introduced to promote the wide applications of teleoperation system, such as amplifying operator's force by choosing a big β. Therefore, the control objectives of teleoperation are transferred into stabilizing e_P and e_F.

Considering Eqs. (1)-(2), the dynamics of position tracking error can be obtained as:

$$\begin{cases} \dot{e}_P = \dot{q}_m l_m - \alpha \dot{q}_s l_s, \\ \ddot{e}_P = \dfrac{l_m \tau_m}{a_m(q_m)} - \dfrac{\alpha l_s \tau_s}{a_s(q_s)} + f_1(t) \end{cases} \tag{8}$$

with

$$f_1(t) = -l_m \frac{\tau_{mext} + f_h l_m + b_m(q_m, \dot{q}_m) + g_m(q_m)}{a_m(q_m)} + \alpha l_s \frac{\tau_{sext} + f_e l_s + b_s(q_s, \dot{q}_s) + g_s(q_s)}{a_s(q_s)}.$$

Similarly, with the definition of e_F in mind, combining Eqs. (1) and (2) yields the force tracking dynamics:

$$\dot{e}_F = \frac{D_h l_m \tau_m}{a_m(q_m)} + \frac{\beta D_e l_s \tau_s}{a_s(q_s)} + f_2(t), \quad s_h > s_m, s_s > s_e \tag{9}$$

with

$$\begin{aligned} f_2(t) &= -D_h l_m \frac{\tau_{mext} + f_h l_m + b_m(q_m, \dot{q}_m) + g_m(q_m)}{a_m(q_m)} \\ &- \beta D_e l_s \frac{\tau_{sext} + f_e l_s + b_s(q_s, \dot{q}_s) + g_s(q_s)}{a_s(q_s)} \\ &+ K_h(\dot{q}_m l_m - \dot{s}_h) + \beta K_e(\dot{q}_s l_s - \dot{s}_e) \\ &- (D_h l_m \ddot{s}_h + \beta D_e l_s \ddot{s}_e). \end{aligned}$$

In this paper, it is assumed that the information of joint positions (q_m and q_s) and joint velocities ($\dot{q}_m$ and $\dot{q}_s$) is available and the contact force f_h and f_e is available. Considering the engineering practice, it is also assumed that there exist perturbations in the model of teleoperation system (1) and (2), and only their nominal model can be obtained. Therefore, the dynamics of position tracking error (8) can be rewritten as:

$$\begin{cases} \dot{e}_P = \dot{q}_m l_m - \alpha \dot{q}_s l_s, \\ \ddot{e}_P = u_P + f_{1n}(t) + d_P(t) \end{cases} \tag{10}$$

with

$$u_P = \frac{l_m \tau_m}{a_{mn}(q_m)} - \frac{\alpha l_s \tau_s}{a_{sn}(q_s)}, \tag{11}$$

$$\begin{aligned} f_{1n}(t) &= -l_m \frac{f_h l_m + b_{mn}(q_m, \dot{q}_m) + g_{mn}(q_m)}{a_{mn}(q_m)} \\ &+ \alpha l_s \frac{f_e l_s + b_{sn}(q_s, \dot{q}_s) + g_{sn}(q_s)}{a_{sn}(q_s)}, \\ d_P(t) &= d_P(q_m, q_s, \dot{q}_m, \dot{q}_s, \tau_m, \tau_s, f_h, f_e, \tau_{mext}, \tau_{sext}), \end{aligned}$$

where $a_{mn}(q_m)$, $a_{sn}(q_s)$, $b_{mn}(q_m, \dot{q}_m)$, $b_{sn}(q_s, \dot{q}_s)$, $g_{mn}(q_m)$, $g_{sn}(q_s)$ are the nominal model of the inertia moment, Coriolis and gravity force torques of master and slave, respectively; u_P is the virtual controller for position tracking. Similarly, the model of contact force tracking error can be rewritten as:

$$\dot{e}_F = u_F + f_{2n}(t) + d_F(t), \quad s_h > s_m, s_s > s_e \tag{12}$$

with

$$u_F = \frac{D_{hn} l_m \tau_m}{a_{mn}(q_m)} + \frac{\beta D_{en} l_s \tau_s}{a_{sn}(q_s)}, \tag{13}$$

$$\begin{aligned} f_{2n}(t) =& - D_{hn} l_m \frac{f_h l_m + b_{mn}(q_m, \dot{q}_m) + g_{mn}(q_m)}{a_{mn}(q_m)} \\ & - \beta D_{en} l_s \frac{f_e l_s + b_{sn}(q_s, \dot{q}_s) + g_{sn}(q_s)}{a_{sn}(q_s)}, \\ d_F(t) =& d_F(q_m, q_s, \dot{q}_m, \dot{q}_s, \tau_m, \tau_s, f_h, f_e, \tau_{mext}, \tau_{sext}), \end{aligned}$$

where D_{hn} and D_{en} are the nominal values of the coefficients; u_F is the virtual controller for force tracking.

The real control action of the teleoperation system is the electrician torques τ_m and τ_s in master and slave robots, and they can be calculated from Eqs. (11) and (13) as:

$$\begin{aligned} \tau_m &= \frac{a_{mn}(q_m)\,(\beta D_{en} u_P + \alpha u_F)}{(\beta D_{en} + \alpha D_{hn}) l_m}, \\ \tau_s &= \frac{a_{sn}(q_s)\,(u_F - D_{hn} u_P)}{(\beta D_{en} + \alpha D_{hn}) l_s}. \end{aligned} \tag{14}$$

It should be noted that the virtual controller u_F in Eq. (13) is defined under the conditions $s_h > s_m$ and $s_s > s_e$, and it is set as $u_F = 0$ when the conditions are not satisfied. It can be verified that the transfer (14) is still established in this case. Therefore, the design of bilateral controller τ_m and τ_s can be transformed to the design of virtual controller u_P and u_F.

3 Controller design and stability analysis

3.1 Enhanced nonlinear disturbance observer design

Assumption 1 The lumped disturbance $d_P(t)$ in position tracking error dynamics (10) is r_1th-order differentiable, and the steady state of its r_1th-order derivative converges to zero, i.e., $\lim_{t\to\infty} d_P^{(r_1)}(t) = 0$.

Assumption 2 The lumped disturbance $d_F(t)$ in force tracking error dynamics (12) is r_2th-order differentiable, and the steady state of its r_2th-order derivative converges to zero, i.e., $\lim_{t\to\infty} d_F^{(r_2)}(t) = 0$.

Lemma 1 *[32] The following single-input linear system:*

$$\dot{\boldsymbol{x}} = \boldsymbol{A}\boldsymbol{x} + \boldsymbol{B}u \tag{15}$$

is asymptotically stable if $\boldsymbol{A}$ is Hurwitz matrix and u is bounded and satisfies $\lim_{t\to\infty} u(t) = 0$.

It is well known that a function in terms of time t can be locally represented by a family of Taylor time polynomial inputs and a residual term. Therefore, the disturbance $d_P(t)$ and $d_F(t)$ in Eqs. (10) and (12) can be represented in the following form as:

$$d_P = \sum_{i=0}^{r_1-1} d_P^i t^i + o_1(t), \quad d_F = \sum_{i=0}^{r_2-1} d_F^i t^i + o_2(t), \tag{16}$$

where $d_P^0, d_P^1, \cdots, d_P^{r_1-1}$ and $d_F^0, d_F^1, \cdots, d_F^{r_2-1}$ are unknown constants; $o_1(t)$ and $o_2(t)$ denote the unknown residual terms. Since d_P^i and d_F^i are assumed unknown, the approximation model (16) can be regard ed as an unknown internal model which can be used to describe a general disturbance.

With the model (16) in mind, the dynamics of disturbances $d_P(t)$ and $d_F(t)$ can be described as:

$$\dot{\boldsymbol{\xi}}_{\boldsymbol{P}} = \boldsymbol{A}_{\boldsymbol{P}}\boldsymbol{\xi}_{\boldsymbol{P}} + \boldsymbol{B}_{\boldsymbol{P}} d_P^{(r_1)}(t), \quad d_P(t) = \boldsymbol{C}_{\boldsymbol{P}}\boldsymbol{\xi}_{\boldsymbol{P}}, \tag{17}$$

$$\dot{\boldsymbol{\xi}}_{\boldsymbol{F}} = \boldsymbol{A}_{\boldsymbol{F}}\boldsymbol{\xi}_{\boldsymbol{F}} + \boldsymbol{B}_{\boldsymbol{F}} d_F^{(r_2)}(t), \quad d_F(t) = \boldsymbol{C}_{\boldsymbol{F}}\boldsymbol{\xi}_{\boldsymbol{F}}, \tag{18}$$

with

$$\boldsymbol{A}_{\boldsymbol{P}} = \begin{bmatrix} 0 & 1 & 0 & \cdots & 0 \\ 0 & 0 & 1 & \cdots & 0 \\ \vdots & \vdots & \vdots & \vdots & \vdots \\ 0 & 0 & 0 & \cdots & 1 \\ 0 & 0 & 0 & \cdots & 0 \end{bmatrix}_{r_1 \times r_1}, \quad \boldsymbol{A}_{\boldsymbol{F}} = \begin{bmatrix} 0 & 1 & 0 & \cdots & 0 \\ 0 & 0 & 1 & \cdots & 0 \\ \vdots & \vdots & \vdots & \vdots & \vdots \\ 0 & 0 & 0 & \cdots & 1 \\ 0 & 0 & 0 & \cdots & 0 \end{bmatrix}_{r_2 \times r_2},$$

$$\boldsymbol{B}_{\boldsymbol{P}} = [0\,0\,\cdots\,0\,1]^T_{1\times r_1}, \quad \boldsymbol{C}_{\boldsymbol{P}} = [1\,0\,\cdots\,0\,0]_{1\times r_1},$$

$$\boldsymbol{B}_{\boldsymbol{F}} = [0\,0\,\cdots\,0\,1]^T_{1\times r_2}, \quad \boldsymbol{C}_{\boldsymbol{F}} = [1\,0\,\cdots\,0\,0]_{1\times r_2},$$

where $\boldsymbol{\xi}_{\boldsymbol{P}} = \begin{bmatrix} \xi_P^1 & \xi_P^2 & \cdots & \xi_P^{r_1-1} & \xi_P^{r_1} \end{bmatrix}^T$ is the internal dynamics of $d_P(t)$, $\boldsymbol{\xi}_{\boldsymbol{F}} = \begin{bmatrix} \xi_F^1 & \cdots & \xi_F^{r_2} \end{bmatrix}^T$ is the internal dynamics of $d_F(t)$. With the disturbance model (17) in mind, the enhanced nonlinear disturbance observers (ENDOBs) [22] for the position and force tracking error system (10) and (12) are designed as:

$$\begin{cases} \dot{\boldsymbol{z}}_{\boldsymbol{1}} = (\boldsymbol{A}_{\boldsymbol{P}} - \boldsymbol{L}_{\boldsymbol{P}}\boldsymbol{C}_{\boldsymbol{P}})\,\boldsymbol{\varepsilon}_{\boldsymbol{1}} - \boldsymbol{L}_{\boldsymbol{P}}\,[u_P + f_{1n}(t)], \\ \boldsymbol{\varepsilon}_{\boldsymbol{1}} = \boldsymbol{z}_{\boldsymbol{1}} + \boldsymbol{L}_{\boldsymbol{P}}\dot{e}_P, \qquad \hat{d}_P = \boldsymbol{C}_{\boldsymbol{P}}\boldsymbol{\varepsilon}_{\boldsymbol{1}}, \end{cases} \tag{19}$$

$$\begin{cases} \dot{\boldsymbol{z}}_{\boldsymbol{2}} = (\boldsymbol{A}_{\boldsymbol{F}} - \boldsymbol{L}_{\boldsymbol{F}}\boldsymbol{C}_{\boldsymbol{F}})\boldsymbol{\varepsilon}_{\boldsymbol{2}} - \boldsymbol{L}_{\boldsymbol{F}}\,[u_F + f_{2n}(t)], \\ \boldsymbol{\varepsilon}_{\boldsymbol{2}} = \boldsymbol{z}_{\boldsymbol{2}} + \boldsymbol{L}_{\boldsymbol{F}}e_F, \qquad \hat{d}_F = \boldsymbol{C}_{\boldsymbol{F}}\boldsymbol{\varepsilon}_{\boldsymbol{2}}, \end{cases} \tag{20}$$

where $\boldsymbol{z}_{\boldsymbol{1}} = [z_1^1\, z_1^2\, \cdots\, z_1^{r_1}]^T$, $\boldsymbol{\varepsilon}_{\boldsymbol{1}} = [\varepsilon_1^1\, \varepsilon_1^2\, \cdots\, \varepsilon_1^{r_1}]^T$, and $\boldsymbol{z}_{\boldsymbol{2}} = [z_2^1\, z_2^2\, \cdots\, z_2^{r_2}]^T$, $\boldsymbol{\varepsilon}_{\boldsymbol{2}} = [\varepsilon_2^1\, \varepsilon_2^2\, \cdots\, \varepsilon_2^{r_2}]^T$ are the virtual state vectors of ENDOBs, z_1^i and ε_1^i with $1 \le i \le r_1$ are the elements of $\boldsymbol{z}_{\boldsymbol{1}}$ and $\boldsymbol{\varepsilon}_{\boldsymbol{1}}$, z_2^i and ε_2^i with $1 \le i \le r_2$ are the elements of $\boldsymbol{z}_{\boldsymbol{2}}$ and $\boldsymbol{\varepsilon}_{\boldsymbol{2}}$, respectively; $\boldsymbol{L}_{\boldsymbol{P}} = [l_P^1\, l_P^2\, \cdots\, l_P^{r_1}]^T$ and $\boldsymbol{L}_{\boldsymbol{F}} = \begin{bmatrix} l_F^1 & l_F^2 & \cdots & l_F^{r_2} \end{bmatrix}^T_{1\times r_2}$, are the observer gain vectors and their elements $l_P^1, \cdots, l_P^{r_1}$ and $l_F^1, \cdots, l_F^{r_2}$ are positive constants.

Theorem 1 *Suppose that Assumptions 1 and 2 are satisfied for systems (10) and (12), the ENDOBs (19) and (20) guarantee the disturbance estimation $\hat{d}_P$ and $\hat{d}_F$ converges to their real values d_P and d_F asymptotically if the observer gains are designed such that the polynomials $s^{r_1} + l_P^1 s^{r_1-1} + \cdots + l_P^{r_1-1} s + l_P^{r_1}$ and $s^{r_2} + l_F^1 s^{r_2-1} + \cdots + l_F^{r_2}$ are Hurwitz.*

Proof Since ENDOBs (19), (20) and disturbance dyn amics (17), (18) have similar formulation, the convergence of ENDOBs (19), (20) is also similar. Without of loss, we choose ENDOB (19) as an example to prove Theorem 1.

Define the disturbance estimation error of d_P as:

$$e_{dP} = \hat{d}_P - d_P.$$

Define the disturbance internal dynamics estimation error as:

$$\begin{aligned} &e_1^i = \varepsilon_1^i - \xi_P^i,\ 1 \le i \le r_1, \\ &\boldsymbol{e_1 = \varepsilon_1 - \xi_P} = [e_1^1\ \cdots\ e_1^{r_1}]^T. \end{aligned}$$

Combining Eqs. (17) and (19) yields:

$$e_{dP} = \varepsilon_1^1 - \xi_P^1 = e_1^1 \tag{21}$$

With Eq. (10) in mind, combining Eqs. (17) and (19) yields:

$$\begin{aligned} \dot{\boldsymbol{e}}_1 &= \dot{\boldsymbol{\varepsilon}}_1 - \dot{\boldsymbol{\xi}}_P \\ &= \dot{\boldsymbol{z}}_1 + \boldsymbol{L_P}\ddot{e}_P - [\boldsymbol{A_P \xi_P} + \boldsymbol{B_P} d_P^{(r_1)}(t)] \\ &= \boldsymbol{A_P(\varepsilon_1 - \xi_P) - L_P C_P \varepsilon_1 + L_P} d_P - \boldsymbol{B_P} d_P^{(r_1)}(t) \\ &= \boldsymbol{(A_P - L_P C_P)(\varepsilon_1 - \xi_P) - B_P} d_P^{(r_1)}(t) \\ &= \boldsymbol{(A_P - L_P C_P) e_1 - B_P} d_P^{(r_1)}(t) \end{aligned}$$

Substituting the values of $\boldsymbol{A_p}$, $\boldsymbol{L_P}$ and $\boldsymbol{C_P}$ into above equations obtains:

$$\dot{\boldsymbol{e}}_1 = \boldsymbol{A_{Pe} e_1 - B_P} d_P^{(r_1)}(t) \tag{22}$$

with

$$\boldsymbol{A_{Pe}} = \begin{bmatrix} -l_P^1 & 1\ 0 \cdots 0 \\ -l_P^2 & 0\ 1 \cdots 0 \\ \vdots & \vdots\ \vdots\ \vdots\ \vdots \\ -l_P^{r_1-1} & 0\ 0 \cdots 1 \\ -l_P^{r_1} & 0\ 0 \cdots 0 \end{bmatrix}.$$

The characteristic equation of system (22) is

$$|s\boldsymbol{I} - \boldsymbol{A_{Pe}}| = s^{r_1} + l_P^1 s^{r_1-1} + \cdots + l_P^{r_1-1} s + l_P^{r_1}. \tag{23}$$

Since the polynomial $s^{r_1} + l_P^1 s^{r_1-1} + \cdots + l_P^{r_1-1} s + l_P^{r_1}$ is Hurwitz, $\boldsymbol{A_{Pe}}$ is a Hurwitz matrix. With Assumption 1 in mind, it concludes from Lemma 1 that $\boldsymbol{e_1}$ converges to zero asymptotically. It deduces from Eq. (21) that e_{dP} is an element of $\boldsymbol{e_1}$, and it also converges to zero asymptotically. Therefore, the disturbance estimation $\hat{d}_P$ converges to its real value d_P asymptotically, which completes the proof.

Remark 2 The order of Taylor polynomial r in Eq. (16) is chosen based on the nature of disturbances $d_P(t)$ and $d_F(t)$. For example, $r = 1$, $r = 2$ and $r = 3$ represent the unknown piecewise constant, slope and parabolic disturbances, respectively. Generally, a larger r means a better approximation and a higher estimation accuracy of the unknown disturbances, but a heavier computation burden is induced simultaneously. Therefore, a tradeoff should be taken into account between the estimation accuracy and the computational burden when designing the ENDOB under the case we have no information of the disturbance's order.

Remark 3 Since the lumped disturbances d_P in (10) and d_F in (12) are multi-source disturbances which include model uncertainties and external disturbances, it is hard to obtain their order. A tradeoff between the estimation accuracy and the computational burden is considered here, and the Taylor polynomial orders r_1 and r_2 in Eq. (16) are chosen as $r_1 = r_2 = 3$ in the simulation part of this paper. In this case, the ENDOBs for Eqs. (10) and (12) degenerate into:

$$\begin{aligned} \dot{z}_{11} =& -l_P^1(z_{11} + l_P^1 \dot{e}_P) - l_P^1[u_P + f_{1n}(t)] \\ &+ z_{12} + l_P^2 \dot{e}_P, \\ \dot{z}_{12} =& -l_P^2(z_{11} + l_P^1 \dot{e}_P) - l_P^2[u_P + f_{1n}(t)] \\ &+ z_{13} + l_P^3 \dot{e}_P, \\ \dot{z}_{13} =& -l_P^3(z_{11} + l_P^1 \dot{e}_P) - l_P^3[u_P + f_{1n}(t)] \\ \hat{d}_P =& z_{11} + l_P^1 \dot{e}_P. \end{aligned} \tag{24}$$

$$\begin{aligned} \dot{z}_{21} =& -l_F^1(z_{21} + l_F^1 e_F) - l_F^1[u_F + f_{2n}(t)] \\ &+ z_{22} + l_F^2 e_F, \\ \dot{z}_{22} =& -l_F^2(z_{21} + l_F^1 e_F) - l_F^2[u_F + f_{2n}(t)] \\ &+ z_{23} + l_F^3 e_F, \\ \dot{z}_{23} =& -l_F^3(z_{21} + l_F^1 e_F) - l_F^3[u_F + f_{2n}(t)] \\ \hat{d}_F =& z_{21} + l_F^1 e_F. \end{aligned} \tag{25}$$

The ENDOBs (24) and (25) guarantee the asymptotical convergence of estimation error when d_P and d_F

are unknown piecewise constants, slopes or parabolic disturbances.

3.2 Bilateral continuous TSM controller design

Design a terminal sliding mode manifold for the position control subsystem (10) as:

$$\sigma = e_P + c_1 |\dot{e}_P|^{\gamma} \operatorname{sign}(\dot{e}_P), \tag{26}$$

where $c_1 > 0$, $\gamma = \frac{p}{q}$, p, q are positive odds and satisfy $q < p < 2q$.

Theorem 2 *For the teleoperation system tracking error dynamics (10) and (12), the following bilateral continuous TSM controller:*

$$\begin{aligned} u_P = &- f_{1n}(t) - \hat{d}_P - \frac{1}{c_1\gamma}|\dot{e}_P|^{2-\gamma}\operatorname{sign}(\dot{e}_P) \\ &- K_P\sigma - \eta_1|\sigma|^{\rho_1}\operatorname{sign}(\sigma), \end{aligned} \tag{27}$$

$$\begin{aligned} u_F = &- f_{2n}(t) - \hat{d}_F - \eta_2|e_F|^{\rho_2}\operatorname{sign}(e_F) \\ &- K_F e_F, \end{aligned} \tag{28}$$

where $\hat{d}_P$, $\hat{d}_F$ are obtained from the ENDOBs (19) and (20), $\eta_1 > 0$, $\eta_2 > 0$, $0 < \rho_1 < 1$, $0 < \rho_2 < 1$, $K_P > 0$ and $K_F > 0$, guarantees the position and force tracking error e_P and e_F converge to the following regions:

$$|e_P| \le 2\delta_1 = 2\min\left\{\frac{|e_{dP}|}{K_P}, \left(\frac{|e_{dP}|}{\eta_1}\right)^{1/\rho_1}\right\}, \tag{29}$$

$$|e_F| \le \delta_2 = \min\left\{\frac{|e_{dF}|}{K_F}, \left(\frac{|e_{dF}|}{\eta_2}\right)^{1/\rho_2}\right\}. \tag{30}$$

The structure of the proposed bilateral continuous terminal sliding model controller is shown in Fig. 3.

3.3 Stability analysis

The proof is divided into two parts: controller (27) guarantees e_P converge to region (29) and controller (28) guarantees e_F converge to region (30).

Part A: finite-time convergence of e_P: The proof is divided into two steps: convergence of sliding variable and convergence of position tracking error.

Step 1: convergence of sliding variable:

With Eqs. (10) and (27) in mind, taking the derivative of sliding variable σ in terms of time yields:

$$\dot{\sigma} = c_1\gamma|\dot{e}_P|^{\gamma-1}[-e_{dP} - \eta_1|\sigma|^{\rho_1}\operatorname{sign}(\sigma) - K_P\sigma \tag{31}$$

Define a Lyapunov function in term of σ as:

$$V_\sigma = \frac{1}{2}\sigma^2. \tag{32}$$

Taking the derivative of V_σ along Eq. (31) yields:

$$\begin{aligned} \dot{V}_\sigma &= -c_1\gamma|\dot{e}_P|^{\gamma-1}\left(\sigma e_{dP} + \eta_1|\sigma|^{\rho_1+1} + K_P\sigma^2\right) \\ &\le -c_1\gamma|\dot{e}_P|^{\gamma-1}\left(\eta_1|\sigma|^{\rho_1} + K_P|\sigma| - |e_{dP}|\right)|\sigma| \\ &= -\bar{c}_1\bar{b}_1 {V_\sigma}^{1/2} \end{aligned} \tag{33}$$

with

$$\bar{c}_1 = c_1\gamma|\dot{e}_P|^{\gamma-1},\ \bar{b}_1 = \sqrt{2}\left(\eta_1|\sigma|^{\rho_1} + K_P|\sigma| - |e_{dP}|\right).$$

We divided the analysis into two cases based on the value of $\dot{e}_P$ in the following part.

1. Case I: $\dot{e}_P \neq 0$
   We have $\bar{c}_1 > 0$ and $\bar{b}_1 > 0$ if σ satisfies:
   $$|\sigma| > \frac{|e_{dP}|}{K_P}, \quad \text{or} \quad |\sigma| > \left(\frac{|e_{dP}|}{\eta_1}\right)^{1/\rho_1}.$$
   Integrating both sides of Eq. (33) yields:
   $$V_\sigma(t)^{1/2} \le V_\sigma(t_0)^{1/2} - \frac{\bar{c}_1\bar{b}_1}{2}(t - t_0),$$
   where $V_\sigma(t_0)$ denotes the initial value of V_σ. Therefore, σ decreases monotonically until it reaches the region:
   $$|\sigma| \le \delta_1, \quad \delta_1 = \min\left\{\frac{|e_{dP}|}{K_P}, \left(\frac{|e_{dP}|}{\eta_1}\right)^{1/\rho_1}\right\}. \tag{34}$$
2. Case II: $\dot{e}_P = 0$
   Substituting the controller (27) into the dynamics of position subsystem (10) yields:
   $$\begin{aligned} \ddot{e}_P = &- e_{dP} - \frac{1}{c_1\gamma}|\dot{e}_P|^{2-\gamma}\operatorname{sign}(\dot{e}_P) - K_P\sigma \\ &- \eta_1|\sigma|^{\rho_1}\operatorname{sign}(\sigma) \\ = &-\operatorname{sign}(\sigma)\left[\frac{e_{dP}}{\operatorname{sign}(\sigma)} + \eta_1|\sigma|^{\rho_1} + K_P|\sigma|\right] \end{aligned}$$
   Both in the cases $|\sigma| > \frac{|e_{dP}|}{K_P}$ and $|\sigma| > (\frac{|e_{dP}|}{\eta_1})^{1/\rho_1}$, we have
   $$K_P|\sigma| + \frac{e_{dP}}{\operatorname{sign}(\sigma)} + \eta_1|\sigma|^{\rho_1} > 0.$$
   It concludes that $\dot{e}_P = 0$ cannot be kept if $|\sigma| > \delta_1$, and once $\dot{e}_P = 0$, $\dot{e}_P$ will change to $\dot{e}_P \neq 0$. This denotes $\dot{e}_P \neq 0$ is always established if $|\sigma| > \delta_1$.

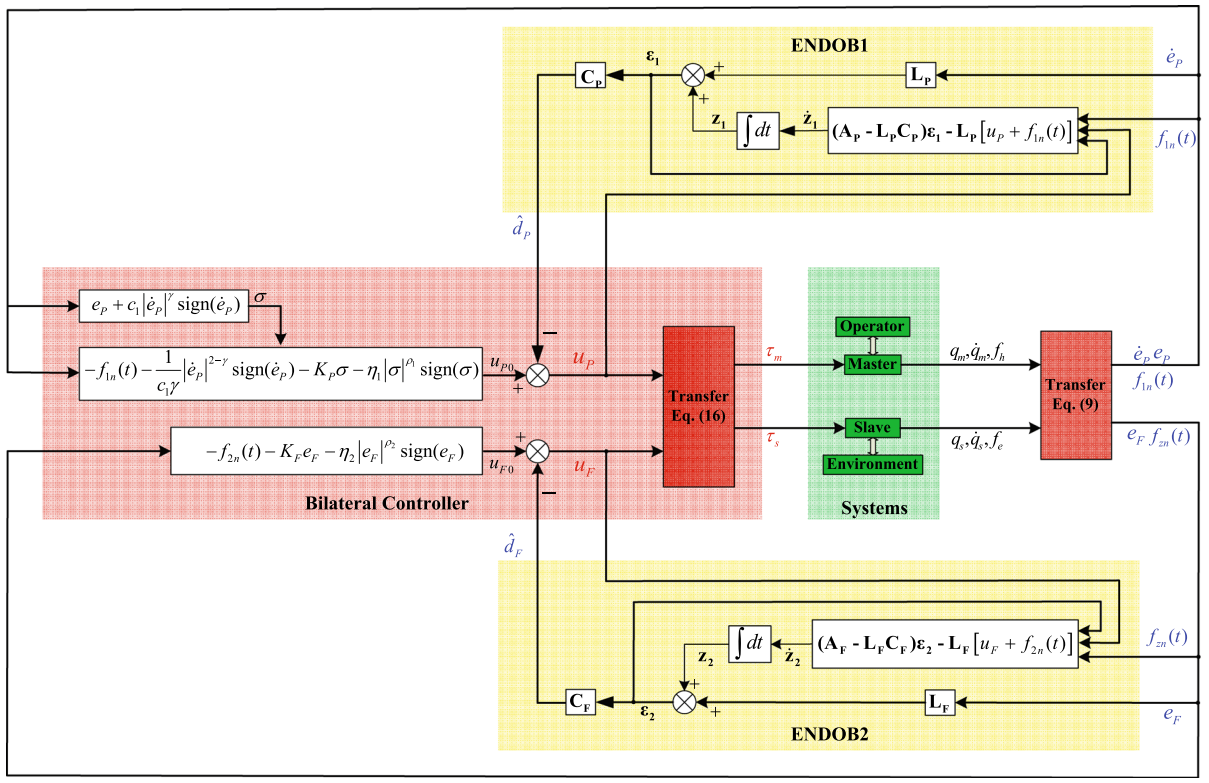

Fig. 3 Block diagram of the bilateral continuous terminal sliding mode controller based on enhanced nonlinear disturbance observer

Therefore, σ converges to the region (34) with a finite time in both of the two cases.

Step 2: convergence of position tracking error: It yields from Eq. (26) that

$$e_P + \Delta|\dot{e}_P|^\gamma \text{sign}(\dot{e}_P) = 0 \tag{35}$$

with

$$\Delta = c_1 - \frac{\sigma}{|\dot{e}_P|^\gamma \text{sign}(\dot{e}_P)}.$$

Considering that $\gamma = p/q$, p, q are positive odds and satisfy $q < p < 2q$, it obtains from Eq. (35) that

$$\dot{e}_P = -\Delta^{-1/\gamma}|e_P|^{1/\gamma}\text{sign}(e_P). \tag{36}$$

After the sliding variable σ reaches the region (34), for the case $|\dot{e}_P| > \left(\frac{\delta_1}{c_1}\right)^{1/\gamma}$, we have

$$\Delta = c_1 - \frac{\sigma}{|\dot{e}_P|^\gamma \text{sign}(\dot{e}_P)} \geq c_1 - \frac{\delta_1}{|\dot{e}_P|^\gamma \text{sign}(\dot{e}_P)} > 0.$$

Let us define a Lyapunov function in terms of e_P as:

$$V_P = \frac{1}{2}e_P^2.$$

Taking the derivative of V_P along Eq. (36) yields

$$\dot{V}_P = -\Delta^{-1/\gamma}|e_P|^{\frac{\gamma+1}{\gamma}} = -2^{\frac{\gamma+1}{2\gamma}}\Delta^{-1/\gamma}V_P^{\frac{\gamma+1}{2\gamma}}.$$

Integrating both sides of the above equation yields:

$$V_P(t)^{\frac{\gamma-1}{2\gamma}} = V_P(t_1)^{\frac{\gamma-1}{2\gamma}} - \bar{\gamma}(t - t_1) \tag{37}$$

with

$$\bar{\gamma} = \frac{\gamma - 1}{2\gamma}2^{\frac{\gamma+1}{2\gamma}}\Delta^{-1/\gamma},$$

where t_1 is the time when the sliding variable σ reaches the region $|\sigma| \leq \delta_1$. Since $1 < \gamma < 2$ and $\Delta > 0$, we have $\bar{\gamma} > 0$. Therefore, it deduces from Eq. (37) that V_P decreases monotonically, which denotes $|e_P|$ decreases monotonically.

It yields from Eq. (36) that $|\dot{e}_P|$ will decrease when $|e_P|$ decreases. Considering that when $\Delta > 0$, $|e_P|$ decreases monotonically, the inequality $|\dot{e}_P| > \left(\frac{\delta_1}{c_1}\right)^{1/\gamma}$ would be broken with time goes on, and this would lead that $\Delta \leq 0$. This means that once $|\dot{e}_P| > \left(\frac{\delta_1}{c_1}\right)^{1/\gamma}$, $\dot{e}_P$ will always converge to the fol-

lowing region:

$$|\dot{e}_P| \leq \left(\frac{\delta_1}{c_1}\right)^{1/\gamma}. \tag{38}$$

With Eq.(38) in mind, it can be deduced from Eq. (26) that

$$|e_P| \leq c_1|\dot{e}_P|^{\gamma} + |\sigma| \leq \delta_1 + |\sigma|.$$

Considering the convergence region of σ in (34) and $\dot{e}_P$ in (38), it yields that e_P will converge to the following region:

$$|e_P| \leq 2\delta_1 = 2\min\left\{\frac{|e_{dP}|}{K_P}, \left(\frac{|e_{dP}|}{\eta_1}\right)^{1/\rho_1}\right\}, \tag{39}$$

which completes the proof of Part A.

Part B: finite-time convergence of e_F: Substituting the controller (28) into the force control subsystem yields:

$$\dot{e}_F = -e_{dF} - \eta_2|e_F|^{\rho_2}\text{sign}(e_F) - K_F e_F. \tag{40}$$

Define a Lyapunov function in terms of e_F as:

$$V_F = \frac{1}{2}e_F^2. \tag{41}$$

Taking the derivative of V_F along Eq. (40) yields:

$$\begin{aligned}\dot{V}_F &= -e_{dF}e_F - \eta_2|e_F|^{\rho_2+1} - K_F e_F^2 \\ &\leq \left(|e_{dF}| - \eta_2|e_F|^{\rho_2} - K_F|e_F|\right)|e_F| \\ &= -\bar{b}_2\sqrt{V_F}\end{aligned} \tag{42}$$

with

$$\bar{b}_2 = \sqrt{2}\left(-|e_{dF}| + \eta_2|e_F|^{\rho_2} + K_F|e_F|\right).$$

We have $\bar{b}_2 > 0$ if e_F satisfy:

$$|e_F| > \frac{|e_{dF}|}{K_F}, \quad \text{or} \quad |e_F| > \left(\frac{|e_{dF}|}{\eta_2}\right)^{1/\rho_2}.$$

In this case, we have

$$\dot{V}_F < -\bar{b}_2\sqrt{V_F} < 0.$$

Integrating both sides of above equation yields:

$$V_F(t)^{1/2} \leq V_F(t_0)^{1/2} - \frac{\bar{b}_2}{2}(t - t_0),$$

where $V_F(t_0)$ denotes the initial value of V_F. Therefore, e_F converges to region (30), which completes the proof.

Remark 4 For the bilateral controllers (27) and (28), if the control parameters of liner terms (i.e., K_P, K_F) and TSM terms (i.e., η_1 and η_2) are chosen the same and big enough:

$$K_P = \eta_1 > |e_{dP}|, \qquad K_F = \eta_2 > |e_{dF}|,$$

the convergence bounds (29) and (30) will decrease to $\delta_1 < 1$ and $\delta_2 < 1$. In this case, the exponential terms $1/\rho_1$ and $1/\rho_2$ will reduce the bound of the convergence region greatly since

$$\left(\frac{|e_{dP}|}{\eta_1}\right)^{1/\rho_1} < \frac{|e_{dP}|}{K_P}, \qquad \left(\frac{|e_{dF}|}{\eta_2}\right)^{1/\rho_2} < \frac{|e_{dP}|}{K_P}.$$

This implies that the proposed controller guarantees smaller convergence bound than linear methods.

4 Simulation study

To validate the effectiveness of the proposed bilateral TSM controller, the simulations on the teleoperation lift robot systems (as shown in Fig. 2) are carried out in this part. Both the master and slave robots are equipped with force sensors to measure the contact force. The model of teleoperation lift robot systems, i.e., the dynamic models of master and slave robots, human operator, and environment, is built based on the SIMULINK-MATLAB software.

4.1 Simulation setting

The inertias and the internal torques due to Coriolis force, external force, and gravity force of master and slave robots in (1) are set based on [30] as:

$$\begin{aligned}&a_m(q_m) = a_{mn}[1 + d_{11}] = 5[1 + 0.1\cos(\pi t)],\\ &b_m(q_m, \dot{q}_m) = b_{mn}[1 + d_{12}] = (-16q_m - 8\dot{q}_m)\\ &[1 - 0.1\sin(\pi t)],\\ &g_m(q_m) = g_{mn}[1 + d_{13}] = 0.5[1 + 0.1\sin(q_m)],\\ &\tau_{mext} = 0.1\sin(2\pi t),\\ &a_s(q_s) = a_{sn}[1 + d_{21}] = 10[1 + 0.2\cos(\pi t)],\\ &b_s(q_s, \dot{q}_s) = b_{sn}[1 + d_{22}] = (-10q_s - 4\dot{q}_s)\\ &[1 + 0.1\cos(2\pi t)],\\ &g_s(q_s) = g_{sn}[1 + d_{23}] = 0.5[1 + 0.1\sin(q_s)],\\ &\tau_{sext} = 0.1\sin(2\pi t),\end{aligned}$$

where a_{mn}, b_{mn}, g_{mn} and a_{sn}, b_{sn}, g_{sn} are the nominal values or functions in master and slave robots dynamics. The model parameters for contact force in (2) are set based on the experimental result in [31] as:

$$D_h = D_{hn}(1 + d_{D_h}) = 25.882(1 + 0.1),$$

$$K_h = K_{hn}(1 + d_{K_h}) = 28683(1 - 0.05),$$
$$D_e = D_{en}(1 + d_{D_e}) = 20(1 - 0.1),$$
$$K_e = K_{en}(1 + d_{K_e}) = 30000(1 + 0.1),$$

where D_{hn}, K_{hn} and D_{en}, K_{en} are the nominal values of the spring and damping coefficients. The distances between the shaft and the point where the contact force is applied are set as $l_m = 0.5$ and $l_s = 0.5$. The parameters for operator dynamics in (4) and environment dynamics in (5) are set as the same with the experimental platform in [31]:

$$M_h = 0.2525,\ k_h = 10.1,\ b_h = 101,\ \lambda_h = 0.5,\ M_e = 80.$$

To demonstrate the lift process more vividly, both the lift and drop cases are considered and the desired position of the operator in (4) is set as:

$$s_h^r(t) = \begin{cases} 0.2(1 - e^{-t}) & 0 \le t < 5, \\ 0.2(1 - e^{t-10}) & 5 \le t < 10. \end{cases}$$

The scaling constants for motion and force in (7) are set as:

$$\alpha = 0.2, \quad \beta = 0.1.$$

The initial vales of positions for operator, master, slave, and environment are set as

$$s_h(0) = 0,\ s_m(0) = 0,\ s_s(0) = 0,\ s_e(0) = 0.$$

To make a tradeoff between the estimation accuracy and the computational burden, the order of Taylor polynomial for d_P and d_F is set as 3. The observer gains for ENDOBs (24) and (25) are set as

$$l_P^1 = 3o_P,\ l_P^2 = 3o_P^2,\ l_P^3 = o_P^3,\ o_P = 100,$$
$$l_F^1 = 3o_F,\ l_F^2 = 3o_F^2,\ l_F^3 = o_F^3,\ o_F = 200.$$

The parameters of controllers (27) and (28) are chosen as

$$\gamma = 5/3,\ c_1 = 5,\ \eta_1 = 10,\ \rho_1 = 0.5,\ K_P = 10,$$
$$\eta_2 = 50,\ \rho_2 = 0.5,\ K_F = 20.$$

Considering the wide existences of control constraints in practical engineering, the real control action of the bilateral lift robot system is set to suffer the following constraints:

$$|\tau_m| \le 500, \quad |\tau_s| \le 500.$$

To make the simulation results more persuasive, simulations under the traditional nonlinear disturbance observer-based composite continuous TSM controller (NDOB based method) and the baseline continuous TSM method without observer (baseline method) are also carried out as comparisons of the proposed method.

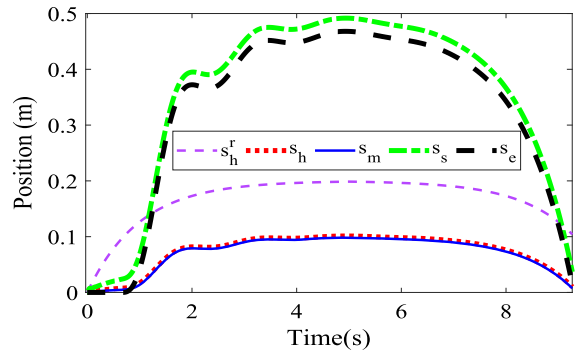

Fig. 4 Position responses of the teleoperation systems

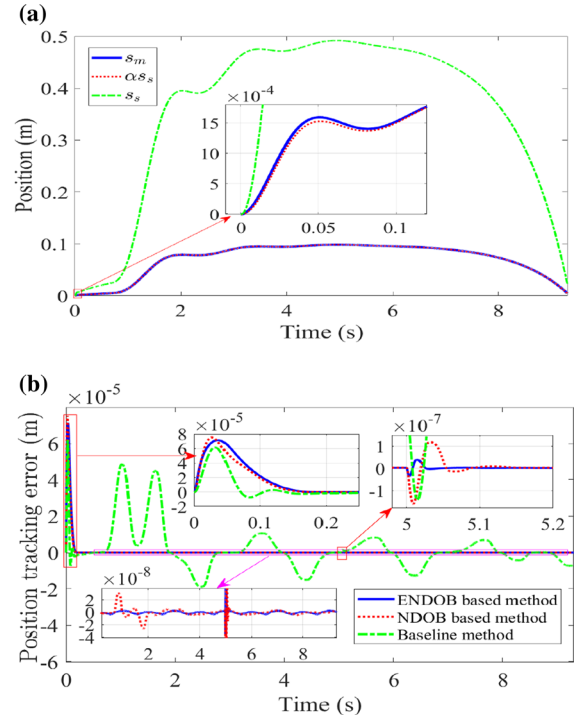

Fig. 5 Response curves of position tracking subsystem: **a** position of master and slave robot s_m and s_s; **b** position tracking error under different methods

4.2 Simulation results and analysis

The simulation results of the teleoperation system under the proposed controller are given in Figs. 4, 5, 6, 7, 8, 9. The position responses of the whole teleoperation system (including operator position s_h, master and slave robots' positions s_m, s_e, environment position s_e, and the desired position of operator s_h^r) are illustrated in Fig. 4. As shown in Fig. 4, the position response curves of the operator s_h and master robot s_m are almost

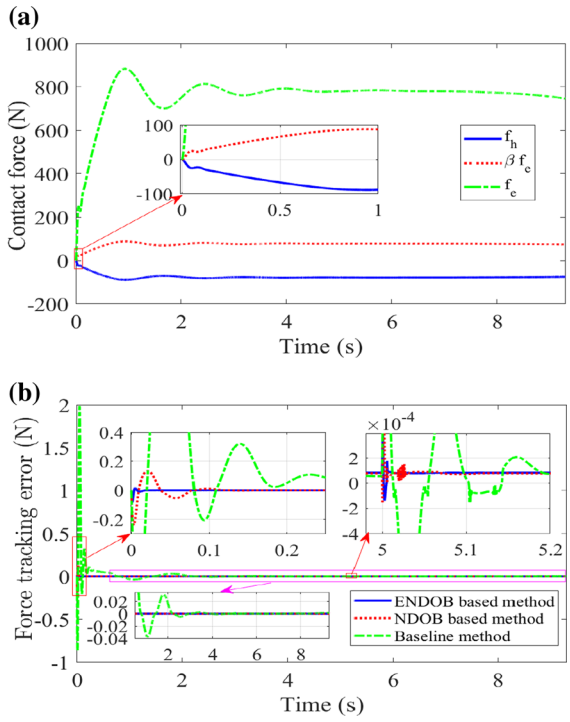

Fig. 6 Response curves of force tracking subsystem: **a** contact force acted on operator and environment f_h and f_e; **b** contact force tracking error under different methods

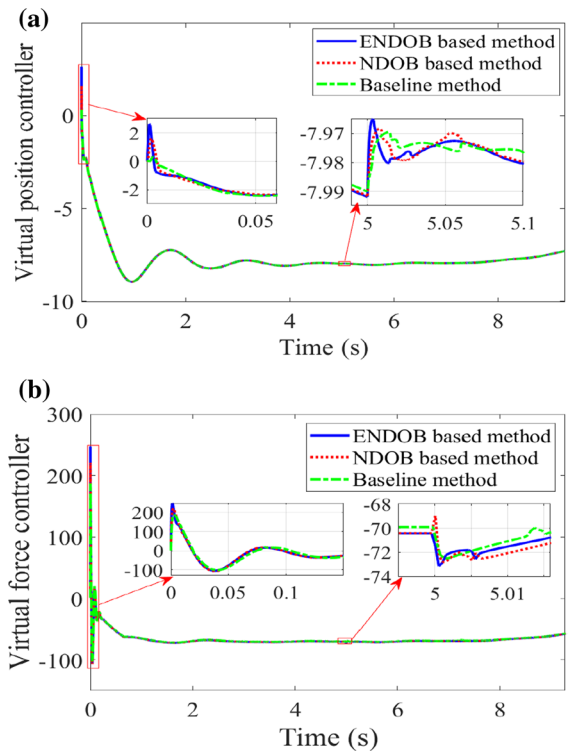

Fig. 7 Response curves of virtual control action: **a** virtual position controller u_P; **b** virtual force controller u_F

the same, and the operator can manipulate the master's position s_m through control its own position s_h, and this verifies the statement in Remark 1. It can be observed that the response curves of the operator's position s_h and its desired position s_h^r are different, while the trend of them is similar. Since the internal control action of the operator f_h^H in Eq. (4) is decided by the feedback of contact force f_h, s_h and s_h^r are not the same. Due to the dynamics of s_h^r being built in the operator, the changing trend of s_h and s_h^r is similar.

Figure 5 demonstrates the control performances of the position control subsystem. Figure 5a shows that the human motion s_m in the local site is transmitted and amplified in the remote site (i.e., s_s). Figure 5b demonstrates the position tracking errors under different methods: (1) both the proposed method and the NDOB-based method guarantee the position tracking error converge to a very small bounded region (less than 5×10^{-8} m), while the convergence bound of the baseline controller is bigger than 2×10^{-5} m; (2) the proposed method has the fastest convergence speed, and this denotes the high precision motion transmission is achieved by the proposed ENDOB based composite continuous TSM bilateral controller.

Figure 6 gives the response curves of the force control subsystem. As shown in Fig. 6a, the operator not only haptics the contact force in the remote site accurately but also realizes the amplify of force in the local site. Figure 6b demonstrates the force tracking error responses under different methods: 1) both the proposed method and the NDOB-based method guarantee the force tracking error converge to a small bounded region (less than 10×10^{-5} N), while the convergence bound of the baseline method is very large; 2) the proposed method guarantees the fastest convergence speed.

Figure 7 demonstrates the response curves of the virtual control action both in position and force tracking subsystem under different methods. It illustrates that the virtual control action in position loop u_P and that in force loop u_F are both continuous under the method. The response curves of real control action (i.e., the electrical torques of the master and slave robots) are demonstrated in Fig. 8. It can be observed from Fig. 7

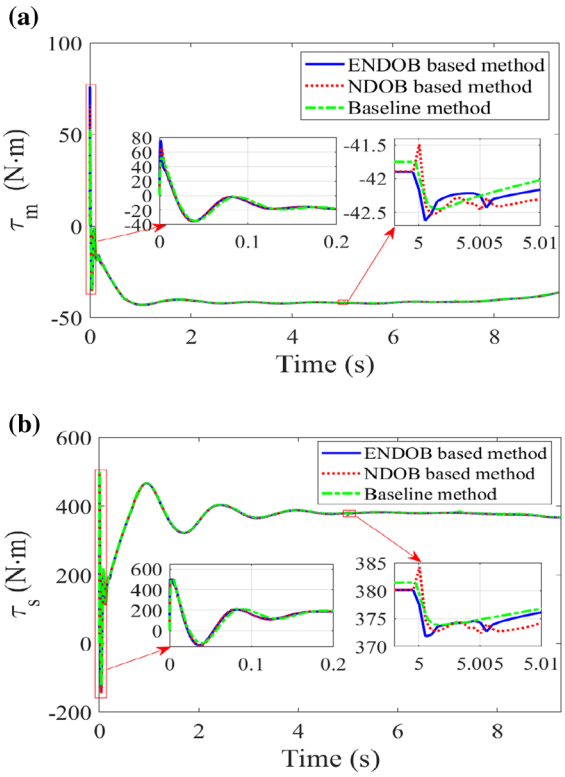

Fig. 8 Response curves of real control action: **a** electrical torque of master robot; **b** electrical torque of slave robot

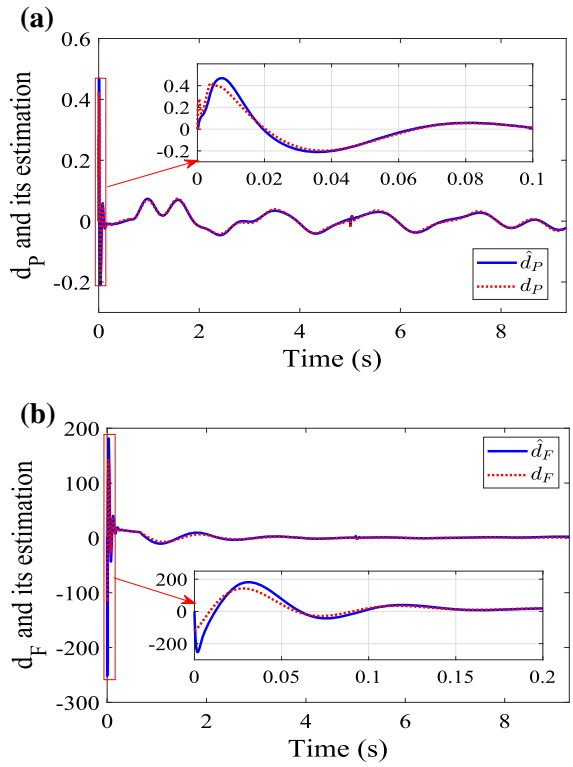

Fig. 9 Disturbance and its estimation: **a** lumped disturbance in position control subsystem d_P and its estimation $\hat{d}_P$; **b** lumped disturbance in force control subsystem d_F and its estimation $\hat{d}_F$

and Fig. 8 that both the virtual control actions and the real control actions under the three methods are guaranteed continuous, and the control level of the three methods is also similar which denotes the fair of the simulation comparisons.

To demonstrate the effectiveness of the proposed ENDOB, the response curves of disturbances in position and force control subsystems and their estimations are given in Fig. 9. It can be found from Fig. 9 that although both of the lumped disturbances d_P in the position subsystem and d_F in the force subsystem are high-order time-varying disturbances, they could be quickly estimated with high precision. Figure 9 also illustrates that the proposed ENDOB achieves high-precision estimation of disturbances even under the case we have no information of disturbance's order, and this verifies the statement in Remark 3.

5 Conclusion

This paper investigates the bilateral control problem of nonlinear teleoperation system with high-order time-varying disturbances. A new enhanced nonlinear disturbance observer (ENDOB) is proposed through employing the Taylor polynomials to approximate the dynamics of unknown high-order time-varying disturbances. And then the composite bilateral controllers are developed based on the estimations of ENDOBs and the continuous terminal sliding mode control methods. The proposed controller not only guarantees the convergence of position and force tracking errors even in the presence of high-order time-varying disturbances but also keeps the continuity of control action. The simulation results on a bilateral lift robot system have

demonstrated the remarkable merits of the proposed controller.

Time delay has huge impact on teleoperation system's stability and transparency [3,33]; we will explore its impact on the bilateral systems in the future research. Considering the wide existence of passivity problem caused by time-delay [34,35], further work would also focus on the handle of passivity problem.

Funding The authors have not disclosed any funding.

Data availability Data sharing is not applicable to this article as no datasets were generated or analyzed during the current study.

Declarations

Conflict of interest The authors declare that there is no conflict of interest.

References

1. Zhao, Y., Liu, P.X., Wang, H., et al.: Funnel-bounded synchronization control for bilateral teleoperation with asymmetric communication delays. Nonlinear Dyn. **107**, 3641–3654 (2022)
2. Yang, Y., Hua, C., Guan, X.: Synchronization control for bilateral teleoperation system with prescribed performance under asymmetric time delay. Nonlinear Dyn. **81**, 481–493 (2015)
3. Chen, H., Liu, Z., Huang, P., Kuang, Z.: Time-delay modeling and simulation for relay communication-based space telerobot system. IEEE Trans. Syst. Man Cybern: Syst. **52**(7), 4211–4222 (2022)
4. SouzanchiK, M., AkbarzadehT, M.R.: Brain emotional learning impedance control of uncertain nonlinear systems with time delay: Experiments on a hybrid elastic joint robot in telesurgery. Comput. Biol. Med. **138**, 104786 (2021)
5. Li, J., You, B., Ding, L., et al.: Dual-master/single-slave haptic teleoperation system for semiautonomous bilateral control of hexapod robot subject to deformable rough terrain. IEEE Trans. Syst. Man Cybern: Syst. **52**(4), 2435–2449 (2021)
6. Li, Y., Liu, K., He, W., et al.: Bilateral teleoperation of multiple robots under scheduling communication. IEEE Trans. Control Syst. Technol. **28**(5), 1770–1784 (2019)
7. Lu, Z., Huang, P., Liu, Z.: High-gain nonlinear observer-based impedance control for deformable object cooperative teleoperation with nonlinear contact model. Int. J. Robust Nonlinear Control **30**(4), 1329–1350 (2020)
8. Mohammadi, L., Alfi, A., Xu, B.: Robust bilateral control for state convergence in uncertain teleoperation systems with time-varying delay: a guaranteed cost control design. Nonlinear Dyn. **88**(2), 1413–1426 (2017)
9. Zhu, W.H., Salcudean, S.E.: Stability guaranteed teleoperation: an adaptive motion/force control approach. IEEE Trans. Autom. Control **45**(11), 1951–1969 (2000)
10. Li, D., Li, P.Y.: Passive bilateral feedforward control of linear dynamically similar teleoperated manipulators. IEEE Trans. Rob. Autom. **19**(3), 443–456 (2003)
11. Sakaino, S., Sato, T., Ohnishi, K.: Precise position/force hybrid control with modal mass decoupling and bilateral communication between different structures. IEEE Trans. Ind. Inf. **7**(2), 266–276 (2011)
12. Ohnishi, K., Ohnishi, K., Miyachi, K.: Torque-speed regulation of dc motor based on load torque estimation. Proceedings of the Institute of Electrical Engineers of Japan Tokyo, 1209–1216 (1983)
13. Sakaino, S., Sato, T., Ohnishi, K.: Multi-dOF micro-macro bilateral controller using oblique coordinate control. IEEE Trans. Ind. Inf. **7**(3), 446–454 (2011)
14. Nozaki, T., Mizoguchi, A., Ohnishi, K.: Decoupling strategy for position and force control based on modal space disturbance observer. IEEE Trans. Ind. Electron. **61**(2), 1022–1032 (2014)
15. Sun, N., Fang, Y., Zhang, X.: Energy coupling output feedback control of 4-DOF underactuated cranes with saturated inputs. Automatica **49**(5), 1318–1325 (2013)
16. Zhai, D., Xia, Y.: Finite-time control of teleoperation systems with input saturation and varying time delays. IEEE Trans. Syst. Man Cybern.: Syst. **40**(7), 1522–1534 (2017)
17. Chen, H., Huang, P., Liu, Z.: Mode switching-based symmetric predictive control mechanism for networked teleoperation space robot system. IEEE/ASME Trans. Mechatron. **24**(6), 2706–2717 (2019)
18. Hace, A., Franc, M.: Pseudo-sensorless high-performance bilateral teleoperation by sliding-mode control and FPGA. IEEE/ASME Trans. Mechatron. **19**(1), 384–393 (2014)
19. Chen, W., Ballance, D.J., Gawthrop, P.J., et al.: A nonlinear disturbance observer for robotic manipulators. IEEE Trans. Ind. Electron. **47**(4), 932–938 (2000)
20. Zhao, Z., Yang, J., Li, S., Chen, W.: Composite nonlinear bilateral control for teleoperation systems with external disturbances. IEEE-CAA J. Automatica Sinica **6**(5), 1220–1229 (2019)
21. Zhao, Z., Yang, J., Liu, C., Chen, W.: Nonlinear composite bilateral control framework for n-DOF teleoperation systems with disturbances. Sci. China-Inform. Sci. **61**(7), 70221 (2018)
22. Chen, W.H.: Disturbance observer based control for nonlinear systems. IEEE/ASME Trans. Mechatron. **9**(4), 706–710 (2004)
23. Dinh, T.N., Defoort, M.: Fixed-time state estimation for a class of switched nonlinear time-varying systems. Asian J. Control **22**(5), 1782–1790 (2020)
24. Bouchama, H.F., Defoort, M., Berdjag, D., Lauber, J.: Design of sliding mode observer for the estimation of train car positions and in-train forces. IFAC-PapersOnLine **54**(4), 98–105 (2021)
25. Mei, K., Ding, S., Yu X.: A generalized super-twisting algorithm. IEEE Trans. Syst. Man Cybern: Cybern. published online https://doi.org/10.1109/TCYB.2022.3188877
26. Ding, S., Zhang, B., Mei, K., Park, T.H.: Adaptive fuzzy SOSM controller design with output constraints. IEEE T. Fuzzy Syst. **30**(7), 2300–2311 (2022)
27. Guo, Z., Guo, J., Wang, X., Chang, J., Huang, H.: Sliding mode control for systems subjected to unmatched distur-

bances/unknown control direction and its application. Int. J. Robust Nonlinear Cont. **31**(4), 1303–1323 (2021)
28. Zhao, Z., Yang, J., Li, S., et al.: Continuous output feedback TSM control for uncertain systems with a DC-AC inverter example IEEE Trans. Circuits-II **65**(1), 71–75 (2017)
29. Ma, Z., Liu, Z., Huang, P., Kuang, Z.: Adaptive fractional-order sliding mode control for admittance-based telerobotic system with optimized order and force estimation. IEEE Trans. Ind. Electron. **69**(5), 5165–5174 (2021)
30. Liu, X., Tao, R., Tavakoli, M.: Adaptive control of uncertain nonlinear teleoperation systems. Mechatronics **24**(1), 66–78 (2014)
31. Fu, M.J., Cavusoglu, M.C.: Human-arm-and-hand-dynamic model with variability analyses for a stylus-based haptic interface. IEEE Trans. Syst. Man Cybern: Cybern. **42**(6), 1633–1644 (2012)
32. Li, S., Yang, J., Chen, W.H., Chen, X.: Generalized extended state observer based control for systems with mismatched uncertainties. IEEE Trans. Ind. Electron. **59**(12), 4792–4802 (2012)
33. Lu, Z., Huang, P., Liu, Z.: Predictive approach for sensorless bimanual teleoperation under random time delays with adaptive fuzzy control. IEEE Trans. Ind. Electron. **65**(3), 2439–2448 (2018)
34. Shen, H., Pan, Y.: Improving tracking performance of nonlinear uncertain bilateral teleoperation systems with time-varying delays and disturbances. IEEE/ASME Trans. Mechatron. **25**(3), 1171–1181 (2019)
35. Chen, Z., Huang, F., Yang, C., Yao, B.: Adaptive fuzzy backstepping control for stable nonlinear bilateral teleoperation manipulators with enhanced transparency performance. IEEE Trans. Ind. Electron. **67**(1), 746–756 (2019)